Heavy ion projectile fragmentation: A reexamination

William A. Friedman
Physics Department, University of Wisconsin, Madison, Wisconsin 53706
(Received 27 August 1982)

We consider the physical effects responsible for the momentum distribution parallel to the beam of nuclides arising from projectile fragmentation. A simple model relates the widths of these distributions to separation energies and an absorptive cutoff radius rather than Fermi momentum. A one-parameter successful treatment of these widths is explored. Coulomb distortions are found to dramatically influence the observed widths at low bombarding energies, leading to a reduction of width with decreasing energy. A simple model for isotope yields from fragmentation reactions is presented and compared with high energy data.

[NUCLEAR REACTIONS Projectile fragmentation of ^{12}C, ^{16}O, ^{20}Ne, $E=2$ GeV/nucleon and $E=10$–20 MeV/nucleon; parallel momentum distribution width; isotope yields.]

I. INTRODUCTION

Several simple characteristics are apparent in heavy ion reactions in which the projectile ion undergoes fragmentation. One of the most striking of these is the peak in the momentum distribution of the fragments near the beam velocity. In this paper we reexamine the essential physics responsible for these peaks, and study the variation of the widths of these peaks with fragment types, projectile, and energy. We will show that many of the general features of both high energy[1] (2 GeV/nucleon) and medium energy[2] (10 MeV/nucleon) fragmentation reactions are well accounted for by simple models for the essential physical features of the reaction.

Let us briefly review the elements of projectile fragmentation theory. The simplest mechanism for these events is represented by the diagram in Fig. 1 which shows a process in which the observed fragment has no interactions with the target. The process involves a virtual breakup of the projectile followed by subsequent interaction of the removed part with the target. In this process the momentum distribution of the fragment is determined by the vertex $|V(k_F)|^2$, which in turn is determined by the ground state projectile wave function. This mechanism is sensitive to the Fermi momentum P_F of the projectile, a quantity also obtainable from electron scattering. Indeed, it is commonly assumed that the observed widths of the momentum distribution are determined by Fermi momentum P_F. A simple model developed by Goldhaber[3] predicts that the width of the fragment momentum distribution parallel to the beam, $\sigma_{||}$, is proportional to the mean momentum of the projectile nucleons and hence directly proportional to the Fermi momentum P_F. Furthermore, Goldhaber showed that the proportionality involves the mass of the fragment, since, for uncorrelated particles, the relationship of the momentum of the fragments to that of the nucleons depends only on this quantity. The relationship is embodied in the following expression for the parallel momentum width[3]:

$$\sigma_{||}=\sigma_0\left[\frac{A_F(A_P-A_F)}{(A_P-1)}\right]^{1/2}, \tag{1.1}$$

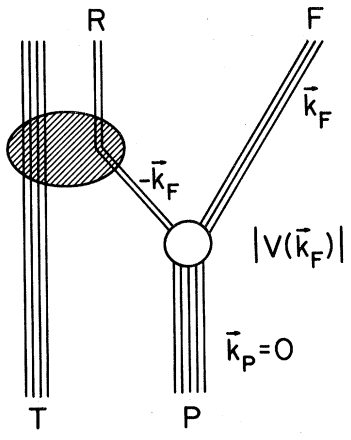

FIG. 1. Schematic diagram for projectile fragmentation process.

where $\sigma_0=P_F/\sqrt{5}$ and A_F and A_P are the fragment and projectile mass numbers. Equation (1.1) predicts that the dependence of $\sigma_{||}$ on fragment mass should follow a parabola peaked at $A_F=\frac{1}{2}A_P$. The experiments with 2 GeV/A ^{16}O projectiles reported in Ref. 1 provide rough agreement with the parabolic behavior with a best fit $\sigma_0=86$ MeV. There is, however, a great deal of scatter of data about the prediction.

The process associated with the diagram in Fig. 1, however, is unable to account for the following: (a) the differences in widths associated with nuclides of the same mass[1]; (b) the discrepancy between σ_0 and $P_F/\sqrt{5}$, where P_F is obtained from electron scattering experiments[1]; (c) the observed difference between $\sigma_{||}$ and $\sigma_\perp$ (Ref. 4); (d) the apparently anomalously small values of σ_0 observed at lower energies[2]; (e) the variation of σ_0 with bombarding energy[2]; and (f) the isotope yields from the fragmentation process.[5] In this paper we present a simple model which deals with each of these shortcomings.

In Sec. II absorption is added, in a qualitative way, to the simple model presented above. The consequence of this change is discussed, and the model is applied to parallel momentum widths from high energy reactions. In Sec. III the question of fragmentation at lower energies is treated and the effect of Coulomb distortion examined. Section IV deals with predictions of isotope yields from fragmentation, and comparison is made with the high energy data. Finally, in Sec. V basic conclusions are summarized.

II. PERIPHERAL MODEL

In this section and the one that follows we develop a model for projectile fragmentation which introduces, in a qualitative way, two essential features missing from the approach taken by Goldhaber in Ref. 3. One of these features, namely, Coulomb distortion, is only significant at lower bombarding energies and is dealt with in the following sections. The other feature, which is important for all bombarding energies, is the subject of this section. Let us call that feature "fragment survival." The requirement of survival dictates that the fragment avoid substantial contact with the target—in other words, the collision must be peripheral. In the language of the optical model, absorptive distortion must be extremely important.

Even when the peripheral nature of the fragmentation reaction is treated only qualitatively, one finds that the Fermi momentum in the projectile can play little role in determining the fragmentation width. The effective absorption prevents the sampling of the entire nucleus, which would be required to establish P_F. Consider the plane wave fragmentation process symbolized by the diagram in Fig. 1. We wish to modify the cross section expression associated with this diagram to include the effect of absorption. For simplicity let us first consider the process in which a single nucleon is removed. For the projectile described by an independent particle model, the vertex for virtual dissociation of the projectile, $|V(\vec{k})|$, is given by

$$|V(\vec{k})|^2 \propto \sum_a |\tilde{\psi}_\alpha(\vec{k})|^2 , \tag{2.1a}$$

$$\tilde{\psi}_\alpha(\vec{k}) \propto \int e^{-i\vec{k}\cdot\vec{r}}\psi_\alpha(\vec{r})d^3\vec{r} , \tag{2.1b}$$

where the wave functions $\psi_\alpha(\vec{r})$ represent nucleon orbits of the projectile. When there is strong absorption, one must introduce an absorption factor in the integrand of Eq. (2.1b). This removes the contribution for small r. Thus, instead of using the Fourier transform of the full wave function for the vertex function, in Eq. (2.1a), one must use the Fourier transform of a cutoff portion of the wave function. While the Fermi momentum is related to the former, it is not to the latter if the cutoff is at a sufficiently large radius.

Let us examine the essential features of absorption through a simple model. Consider a wave function $\psi_{F-R}(r)$ which describes the relative separation between the observed fragment (F) and the removed portion of the projectile (R). In fact, we only need to know the portion of this wave function outside of the absorption region, i.e., far from the center, where

$$\psi_{F-R}(r)\simeq e^{-\mu r}/r , \tag{2.2a}$$

$$\mu=\sqrt{2m_rE_s} , \tag{2.2b}$$

with m_r the reduced mass and E_s the separation energy.

To obtain the width of the fragmentation momentum distribution parallel to the beam direction (taken as z here), we must evaluate

$$V(k_{||})\sim \int e^{-ik_{||}z}F(\vec{r}_\perp,z)\psi(\vec{r}_\perp,z)dz\,dr_\perp^2 , \tag{2.3}$$

where $F(r)$ damps the central portion of the integrand.

In Fig. 2 we show a schematic sketch of the magnitude $|F(\vec{r})\psi(\vec{r})|$ for $z=0$ with the perpendicular direction labeled $r_\perp$. In order to evaluate Eq. (2.3), we require the z dependence of $F\psi$. Because of the absorption indicated in Fig. 2, we expect to find the largest contribution to the integrand near the point $r_\perp=x_0$ and $z=0$. We thus expand r to lowest order in z about this point to obtain

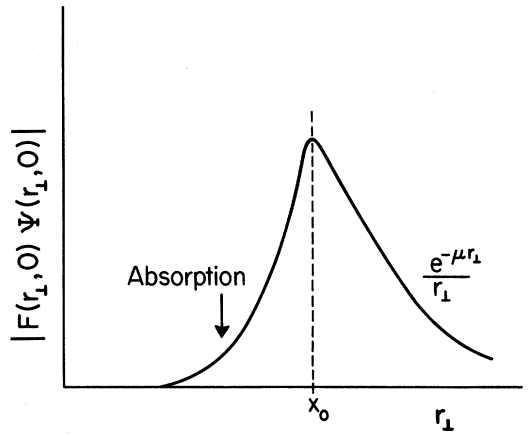

FIG. 2. Schematic plot of $|F(\vec{r})\psi(\vec{r})|$ for $z=0$ as a function of $r_\perp$.

$$F(\vec{r})\psi(\vec{r}) \sim \left[\frac{e^{-\mu z^2/2x_0}}{(1+z^2/x_0^2)^{1/2}} \right] f(r_\perp) . \tag{2.4}$$

The approximate form of Eq. (2.4) permits a separation of the integration variables in the Fourier integral, Eq. (2.3), and provides

$$|V(k_{||})|^2 \approx e^{-(1/2)k_{||}^2/\sigma_{||}^2} , \tag{2.5}$$

with

$$\sigma_{||}^2 = \frac{\mu}{2x_0} \left[1+\frac{1}{\mu x_0} \right] . \tag{2.6}$$

We associate this width with the parallel momentum distribution arising in the fragmentation process. Note that in this approach $\sigma_\perp$ (not treated here) is, in general, different from $\sigma_{||}$ and depends in detail on the shape of the absorption.

We can modify the expression for $\sigma_{||}$ obtained in Eq. (2.6) to include the lowest order effect of the Coulomb potential on the bound state wave function tail. This is accomplished through a Wentzel-Kramers-Brillouin (WKB) approximation to the wave function,

$$\psi(r) \sim \frac{e^{-[2m_r(E_s+Z_1Z_2e^2/r)]^{1/2}r}}{r} , \tag{2.7}$$

which gives

$$\sigma_{||}^2 = \frac{\mu}{2x_0} \left[\frac{1+\frac{1}{2}y}{\sqrt{1+y}} + \frac{1}{\mu_0 x_0} \right] , \tag{2.8}$$

where μ is given by Eq. (2.2b) and

$$y = Z_1Z_2e^2/x_0E_s .$$

The expressions for $\sigma_{||}$ in Eq. (2.8) depend on two primary features, E_s and x_0, i.e., the cluster separation energy and the cutoff radius related to the fragment size. One can easily obtain ground state separation energies from mass tables. This sets a lower bound on E_s. On the other hand, the fragment will be observed if the process leads to any of its particle-stable excited states. This possibility provides a range and upper value for E_s. To deal with x_0 in a systematic way, let us assume that for each fragment with mass number A_F, $x_0 = r_0 A_F^{1/3}$, where r_0 is parameter-independent of the fragment type.

We have examined the fragmentation data of Ref. 1 which involve about 40 different fragments. Using the upper limit for E_s, we find that a single value of $r_0 \approx 1.2$ accounts well for both carbon and oxygen projectile data. Note that while the predictions are for primary distributions without initial or final state inelasticity, the data include possible inelasticity and products of secondary decay. The value of $r_0 = 1.2$ is also obtained if we consider those fragments which are not likely to be the product of secondary decay.

The predicted values of $\sigma_{||}$ for the fragments of ^{12}C are shown in Table I, along with the experimental values of Ref. 1 and the Goldhaber prediction for which σ_0 is set to give the single nucleon removal width. The agreement between prediction and data is excellent. Similar results are shown for the fragmentation of ^{16}O in Table II. For these the agreement is qualitative, but not as good as for carbon.

TABLE I. Widths of the momentum distributions parallel to the beam for fragments from ^{12}C projectiles.

Isotope	$\sigma_{||}$ exp[a] MeV/c	$\sigma_{||}$ theory[b] MeV/c	$\sigma_{||}$[b] Goldhaber MeV/c
^{11}C	103±4	103	103
^{10}C	121±6	125	138
^{9}C	147±21	149	161
^{11}B	106±4	102	103
^{10}B	134±3	120	138
^{8}B	151±16	154	175
^{10}Be	129±4	124	138
^{9}Be	133±3	128	161
^{7}Be	145±2	143	183
^{9}Li	161±9	146	161
^{8}Li	159±7	152	175
^{7}Li	144±2	142	183
^{6}Li	127±7	149	186

[a]Reference 1.
[b]Equation (2.8) with $r_0 = 1.2$.
[c]Goldhaber (Ref. 3) with $\sigma_0 = 103$.

TABLE II. Widths of momentum distributions parallel to the beam for fragments from ^{16}O projectiles.

Isotope	$\sigma_{\parallel}$ exp[a] MeV/c	$\sigma_{\parallel}$ theory[b] MeV/c	$\sigma_{\parallel}$[b] Goldhaber MeV/c
^{15}O	94±3	94	94
^{14}O	99±6	113	128
^{13}O	143±14	141	151
^{15}N	95±3	94	94
^{14}N	112±3	112	128
^{13}N	134±2	120	151
^{12}N	153±11	146	168
^{14}C	125±3	114	128
^{13}C	130±3	121	151
^{12}C	120±4	109	168
^{11}C	162±5	142	179
^{10}C	190±9	154	188
^{9}C		172	192
^{13}B	166±10	137	151
^{12}B	163±8	145	168
^{11}B	160±2	142	179
^{10}B	175±7	147	188
^{8}B	175±22	168	194
^{12}Be		153	168
^{11}Be	197±20	162	179
^{10}Be	159±6	155	188
^{9}Be	166±7	150	192
^{7}Be	166±2	157	192
^{9}Li	188±15	172	192
^{7}Be	166±2	157	192
^{9}Li	188±15	172	192
^{8}Li	170±13	169	194
^{7}Li	167±4	158	192
^{6}Li	141±7	159	188

[a]Reference 1.
[b]Equation (2.8) with $r_0=1.2$.
[c]Goldhaber (Ref. 3) with $\sigma_0=94$.

We shall make further comments on this difference in the discussion in Sec. IV which deals with isotope yields.

In recent detailed calculations for single-particle removal, Hüfner and Nemes[6] reached conclusions similar to ours with regard to the importance of absorption. Their work has been limited to a specific reaction and rests on the construction of the Wigner "distribution" function $W(\vec{R},\vec{k})$ for interpretation. The approach here is global in nature with emphasis on the qualitative features perceived essential. It seems to us that the most straightforward interpretation of the physics may be clouded by the construction of the Wigner function, since the interpretation of this function is itself murky and since construction of this function requires knowledge of the wave function everywhere, even in the absorbed region. At the level of the simplifying assumptions made above, the formalism of Hüfner and Nemes reduces to one similar to ours for the case of single nucleon removal.

Let us now examine why the nonabsorptive, plane wave approach can give results similar to those of the peripheral approach taken here. This must arise from the relationship between Fermi energy E_F and separation energy E_s. For nuclear matter it is argued that the average binding energy and the separation energy are equal.[7] This requires that one introduce an effective mass m^*. If one takes $m^*\approx 0.5$, the ratio of E_F/E_s is 4 to 5. For light, finite nuclei one empirically finds that E_F/E_S is 2 to 3.

Consider the expression in Eq. (2.6) for the momentum width associated with single neutron removal. If we define the ratio of separation energy to Fermi energy, E_s/E_F, as β, then we can express $\sigma_{\parallel}^2$ in terms of this quantity:

$$\sigma_{\parallel}^2=\frac{P_F^2}{5}\frac{2.5}{x_0P_F}\left[\sqrt{\beta}+\frac{1}{x_0P_F}\right]. \tag{2.9}$$

For the fragment coming from ^{16}O the value of x_0P_F is approximately 4, and β is approximately 0.5 when excited states are included in E_s. With this numerical value Eq. (2.9) provides the following results:

$$\sigma_{\parallel}\sim\frac{0.8P_F}{\sqrt{5}}. \tag{2.10}$$

We can thus understand the similarity between the predicted magnitudes for $\sigma_{\parallel}$ from the two approaches. The parabolic fragment mass dependence, explicitly found in Ref. 3, arises here implicitly as a result of the fact that E_s is roughly proportional to the mass number of the removed portion of the projectile times the separation energy of the single nucleon.

III. LOWER ENERGY FRAGMENTATION

In the preceding section we were concerned with the interpretation of high energy data, where one might expect the process of projectile fragmentation to be most pronounced. At what energy does the process become important? This is a topic of current interest and debate. With the measurement of narrow widths σ_0 at 10–20 MeV (Ref. 2) it has been suggested that the simple fragmentation widths are not seen at these energies. This conclusion is based on the presumption that the asymptotic σ_0 is of the order of 90 MeV/c, i.e., that expected from the Fermi energy ($P_F/\sqrt{5}$). In the peripheral model discussed above, σ_0 defined in Eq. (1.1) has no particular physical meaning. Marked variations in this quantity are observed for specific fragments. Be-

cause of the widespread use of σ_0 in the literature, however, we will discuss widths $\sigma_{||}$ (the physically meaningful quantity) in terms of this reduced quantity σ_0 by defining σ_0:

$$\sigma_0 \equiv \sigma_{||} \left[\frac{(A_p - 1)}{(A_F)(A_p - A_F)} \right]^{1/2} . \tag{3.1}$$

At lower energies we must consider a second important distortion, that due to the Coulomb force. This force will have the effect of reducing the width of the parallel momentum distribution at the detector. This is seen by the following simple schematic demonstration.

Consider a high energy beam with emission along the beam direction. Take $\vec{v}_i$ and $\vec{v}_f$ to be the velocity of the emitted fragment before and after acceleration from the Coulomb field. The two velocities can be written as

$$\vec{v}_i = \vec{v}_{0i} + \vec{\eta}_i , \tag{3.2a}$$

$$\vec{v}_f = \vec{v}_{0f} + \vec{\eta}_f , \tag{3.2b}$$

where $\vec{v}_{0i}$ and $\vec{v}_{0f}$ are the velocities of the centroids of the fragment distributions and $\vec{\eta}_i$ and $\vec{\eta}_f$ represent deviations from these centroids before and after Coulomb acceleration. The centroid velocities are related by the Coulomb energy shift E_C,

$$v_{0i}^2 = v_{0f}^2 - \frac{2E_C}{M} . \tag{3.3}$$

The observed distribution in v_f is assumed to come from an original fragmentation distribution in v_i, which we take to be Gaussian with width σ_i,

$$e^{-\eta_i^2/2\sigma_i^2} .$$

The initial and final velocities are related by the Coulomb shift, so we obtain from Eqs. (3.2) and (3.3)

$$2\vec{\eta}_i \cdot \vec{v}_{0i} + \eta_i^2 = 2\vec{\eta}_f \cdot \vec{v}_{0f} + \eta_f^2 .$$

For $\vec{\eta}_i$ and $\vec{\eta}_f$ along $\vec{v}_0$, and $\eta_i \ll v_{0i}$, we have

$$\eta_i = \eta_f / (v_{0i}/v_{0f}) .$$

Thus $e^{-\eta_i^2/2\sigma_i^2}$ becomes $e^{-\eta_f^2/2(\sigma_i v_{0i}/v_{0f})^2}$ and the observed width σ_f is given by

$$\sigma_f = \sigma_i \frac{v_{0i}}{v_{0f}} . \tag{3.4}$$

If the fragment and the projectile have the same charge to mass ratios,

$$\sigma_f \cong \sigma_i (1 - E_{C0}/E_0)^{1/2} , \tag{3.5}$$

where E_0 is the beam energy and E_{C0} is the kinetic energy reduced due to the Coulomb potential for the incoming projectile. A calculation which exactly treats the Coulomb distortions by taking classical trajectories for the fragments produced at the edge of the target nucleus displays qualitative agreement with the results of the simple estimate given in Eq. (3.4).

TABLE III. Widths σ_0 for momentum distributions parallel to the beam for ^{16}O fragments from ^{20}Ne projectiles at various energies.

E/nucleon	σ_0[a]
∞	49
20	41
14.5	37
11.0	34
7.5	26

[a]From Eq. (2.8) with Coulomb corrections.

Now let us examine those recent data which show great deparatures from $\sigma_0 \cong 90$. We specifically consider the data[2,8] for $^{20}\text{Ne} + {}^{197}\text{Au} \rightarrow {}^{16}\text{O} + X$, $^{20}\text{Ne} + {}^{197}\text{Au} \rightarrow {}^{12}\text{C} + X$, and $^{16}\text{O} + {}^{197}\text{Au} \rightarrow {}^{12}\text{C} + X$ in the range from 7 to 20 MeV/nucleon.

First note that one would expect small values for σ_0 due to the low separation energies for α clusters. In fact, in $^{16}\text{O} + {}^{208}\text{Pb} \rightarrow {}^{19}\text{C} + X$ at 2 GeV, a value for σ_0 of 67 MeV/c is extracted from the data, while peripheral model calculations would predict a width of about 60 MeV/c.

When the peripheral model is applied to ^{20}Ne with r_0 set at 1.2 (the value required for the fragments in ^{16}O and ^{12}C experiments), we predict $\sigma_0 = 49$ MeV/c for $^{20}\text{Ne} \rightarrow {}^{16}\text{O}$. If, in addition, we consider the Coulomb distortion, we predict the variation σ_0 with beam energy shown in Table III. Note that both the magnitude and the variation with energy are in agreement with the data of Ref. 2.

For the case of $^{20}\text{Ne} \rightarrow {}^{12}\text{C}$ the peripheral model predicts $\sigma_0 = 57$. Using the same Coulomb reduction as for the ^{16}O fragments we obtain the widths given in Table IV. These values are also in good

TABLE IV. Widths σ_0 for momentum distributions parallel to the beam for ^{12}O fragments from ^{20}Ne projectiles at various energies.

E/nucleon	σ_0[a]
∞	57
20	47
14.5	43
11	40
7.5	30

[a]From Eq. (2.8) with Coulomb corrections.

agreement with the observations. The ratio of widths for ^{12}C and ^{16}O fragments is predicted to be 1.163. This ratio is what is found experimentally for all the energies greater than 10 MeV/nucleon.

Finally, let us examine the results for carbon fragments from oxygen projectiles reported by the Berkeley group.[8] As noted above, the peripheral model predicts a value for σ_0 of 60 MeV/c before Coulomb distortion. The Coulomb modifications give the predictions shown in Table V, which are in good agreement with the results of Ref. 7.

In closing this section, we draw three conclusions: (a) the agreement between the peripheral model predictions and experimental data is remarkable at energies in the range of 10–20 MeV/nucleon; (b) the small size of σ_0 is no indication of the absence of a simple fragmentation process; (c) the observed energy variation of σ_0 between 10 and 20 MeV/nucleon is similar for the three cases discussed above, and this variation is consistent with that expected from Coulomb distortion.

IV. ISOTOPE YIELDS

In this section we extend the peripheral model in order to qualitatively predict nuclide yields arising from projectile fragmentation processes.

For the model of projectile fragmentation we have been considering, we would expect the isotope yields to be characteristic of the projectile but not the target. In experiments with ^{16}O at 2.1 GeV/u and ^{12}C ^{12}C at 2.1 and 1.05 GeV/u, Lindstrom *et al.*[4] employed a wide range of target nuclei. Their analysis of the data assumed that the cross section could be written as

$$\sigma_{PT}^{F}=\gamma_{P}^{F}\gamma_{T} , \tag{4.1}$$

where P, F, and T refer to the projectile, fragment, and target, respectively. They report $\gamma_T \cong A_T^{1/4}$ and claim that this supports the view that the reaction is occurring at the surface. They also present a set of factors γ_P^F from data on all of the targets. These factors provide the relative yield of fragments from a given projectile.

TABLE V. Widths σ_0 for momentum distributions parallel to the beam for ^{12}C fragments from ^{16}O projectiles at various energies.

E/nucleon	σ_0[a]
∞	60
20	48
14.5	46
11.0	42
7.5	31

[a]From Eq. (2.8) with Coulomb corrections.

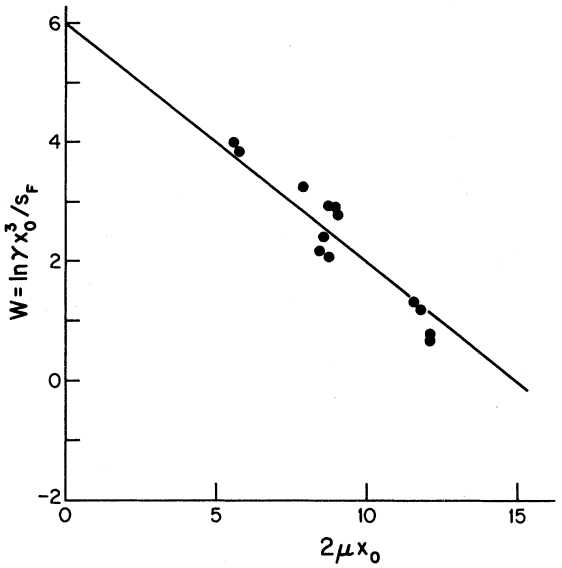

FIG. 3. $W[=\ln(\gamma_P^F x_0{}^3/S_F)]$ vs $2\mu_F x_{0_F}$ for fragments from ^{12}C. γ_P^F from Ref. 5.

We now extend the peripheral model discussed in the previous section so as to be able to predict the relative values of γ_P^F.

We assume that the fragment (F) and part removed from the projectile (R) are described by the relative wave function

$$\psi_{F-R}(r)=\sqrt{S_F}\tilde{\psi}_{F-R}(r) , \tag{4.2}$$

where $\tilde{\psi}_{F-R}$ is normalized to unity and S_F (Ref. 9) is a spectroscopic factor.

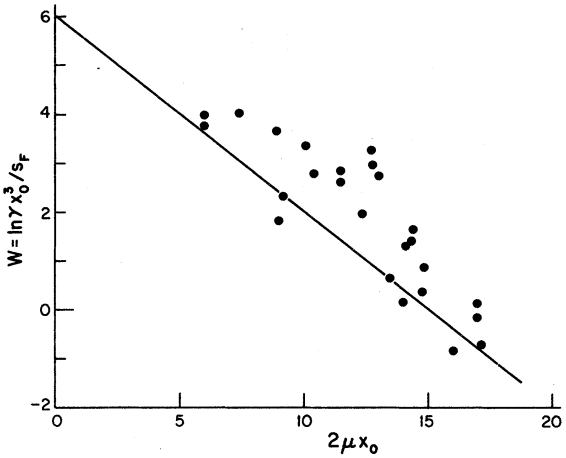

FIG. 4. $W[=\ln(\gamma_P^F x_0{}^5/S_F)]$ vs $2\mu_F x_0$ for fragments from ^{16}O. γ_P^F from Ref. 5.

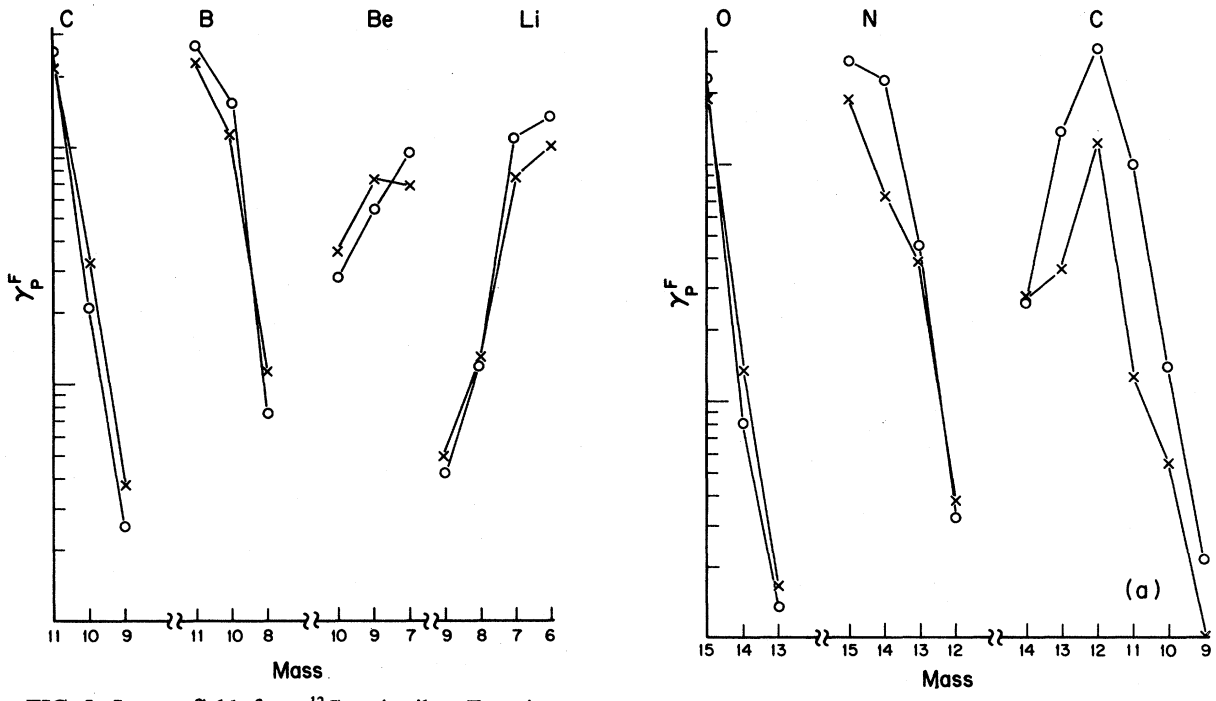

FIG. 5. Isotope fields from ^{12}C projectiles. Experimental data (Ref. 5) (circles); prediction (crosses) from Eq. (4.8) with $b=0.4$.

Let us assume that γ_p^F is given by

$$\gamma_P^F \propto S_F \,|\, \tilde{\psi}_{R-F}(x_{0_F}) \,|^2 , \tag{4.3}$$

where x_{0_F} is that cutoff radius which was used to obtain reasonable fits to the fragmentation widths, i.e., $x_{0_F}=1.2A_F^{1/3}$.

In estimating S_F let us take the relative probability for finding together the necessary protons (Z_R) and neutrons (N_R) which must be removed from the projectile to produce the fragment. Let us thus take S_F to be given by

$$S_F = S_F(Z_R,N_R) \Big/ \sum_{N_R+Z_R=A_R} S_F(Z_R,N_R) , \tag{4.4a}$$

where A_R is the mass number of the particles removed for the fragment and the function $S_F(Z_R,N_R)$ is given by

$$S_F(Z_R,N_R) = \frac{Z_P!N_P!}{Z_R!Z_F!N_R!N_F!} . \tag{4.4b}$$

For

$$|\, \tilde{\psi}_{R-F}(x_{0_F}) \,|^2$$

we take

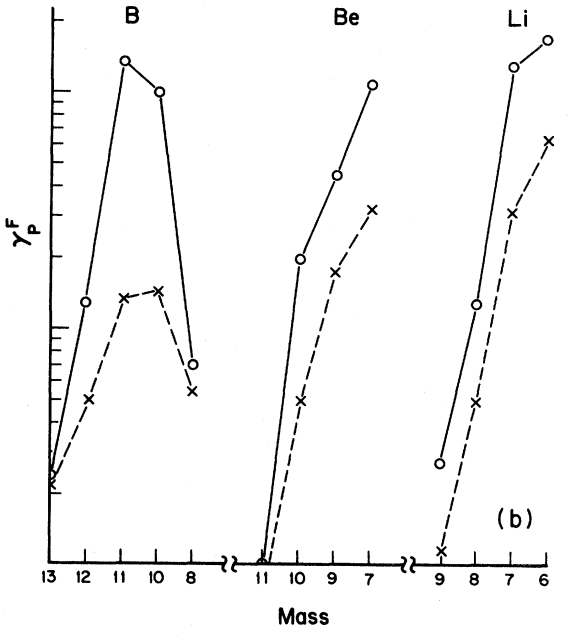

FIG. 6. Isotope yields from ^{16}O projectiles. Experimental data (Ref. 5) (circles); prediction (crosses) from Eq. (4.8) with $b=0.4$.

$$N_F{}^2 e^{-2\mu_F x_{0_F}}/x_{0_F}{}^2$$

and express the normalization in $N_F{}^2$ as follows:

$$N_F{}^2 = \frac{e^{2\mu_F R_{c_F}}}{R_{c_F}} . \tag{4.5}$$

Here R_{c_F} is a central radius, less than x_{0_F}, which provides the normalization. This form for $N_F{}^2$ would arise for a wave function constant up to $r = R_c$, exponentially falling for $r > R_c$. Combining Eqs. (4.3)—(4.5), we obtain

$$\gamma_P^F \propto \frac{S_F e^{-2\mu_F(x_{0_F} - R_{c_F})}}{x_{0_F}{}^2 R_{c_F}} . \tag{4.6}$$

Let us further assume that R_{c_F} varies only with the fragment size $A_F{}^{1/3}$, so that R_{c_F} is proportional to x_{0_F}. Let us take this proportionality factor equal to $(1-b)$ and independent of fragment mass,

$$R_{c_F} = (1-b) x_{0_F} . \tag{4.7}$$

With Eqs. (4.6) and (4.7) we obtain

$$\gamma_P^F \propto S_F \frac{e^{-2\mu_F x_{0_F} b}}{x_{0_F}{}^3 (1-b)} . \tag{4.8}$$

In this expression everything but b is assumed known: μ_F is obtained from separation energies; $x_{0_f} = 1.2 A_F{}^{1/3}$; and S_F is constructed from Eq. (4.4b).

It is convenient to consider the following equation for the function

$$W(\equiv \ln \gamma_P^F X_{0_F}{}^3 / S_F)$$

which arises from Eq. (4.8):

$$W \equiv \ln \left[\frac{\gamma_P^F x_{0_F}{}^3}{S_F} \right]$$

$$= -b(2\mu_F x_{0_F}) - \ln(1-b) + \text{const} . \tag{4.9}$$

A plot of W versus $(2\mu_F x_{0_F})$ for the fragments of a given projectile would provide a straight line with slope b if the model outlined above were valid. As seen in Fig. 3, this is indeed the case found for the ^{12}C results—the projectile where the width predictions were best. The results for ^{16}O, displayed in Fig. 4, show a strong correlation but more scatter than in the case for ^{12}C. From the slope of the curve in Fig. 3 we find $b = 0.4$ or $R_{c_F} = 0.6 x_{0_F}$. The same value of slope seems consistent with the ^{16}O results.

Let us return to Eq. (4.8) and set $b = 0.4$ in order to obtain predictions for γ_P^F. This follows with the choice of a single overall normalization factor.

The predictions for γ_P^F for both the ^{16}O and the ^{12}C projectiles have been generated. These are plotted versus isotope in Figs. 5 and 6. For comparison the experimental data (γ_P^F) from Ref. 4 are also indicated. The results are remarkably good for the ^{12}C case. For ^{16}O the largest deviations come where one might expect secondary decays to be important in populating the isotopes yields. The fact that the width predictions were less good for ^{16}O is also consistent with yield coming from secondary decay.

V. CONCLUSIONS

We have reexamined the high energy fragmentation process incorporating the feature of fragment survival or peripherality. This approach suggests that the separation energy E_s, and not the Fermi momentum P_F, is crucial in determining the parallel momentum widths. We can achieve general agreement between predictions and experimental data by setting one parameter, r_0, to the value 1.2 fm. We are currently examining ways of obtaining more meaningful primary distributions which take account of inelasticity. These distributions should be compared with Eq. (2.8) to determine r_0. Preliminary results indicate a single value in the range $2 > r_0 > 1.2$ may be consistent with these modifications. This will be the subject of a subsequent report.

We have applied the peripheral model to data at lower energies (10—20 MeV/nucleon). In these cases, it is important to incorporate the effect of Coulomb distortion. This leads to agreement with the observed narrow widths. The inclusion of Coulomb distortion also provides a simple explanation for the energy variation of the widths between 10 and 20 MeV.

Finally, with additional assumptions, we have obtained predictions of the isotope yields from high energy reactions which are consistent with experimental data. The agreement between theory and experiment is best when the momentum widths are best predicted—a gratifying correlation.

ACKNOWLEDGMENTS

The author appreciatively acknowledges the hospitality of the National Superconducting Cyclotron Laboratory at Michigan State University where most of the work was performed. The project was supported in part by the National Science Foundation.

[1]D. E. Greiner, P. J. Lindstrom, H. H. Heckman, B. Cork, and F. S. Bieser, Phys. Rev. Lett. 35, 152 (1975).

[2]Ch. Egelhaaf, G. Bohlen, H. Fuchs, A. Gamp, H. Homeyer, and H. Kluge, Phys. Rev. Lett. 46, 318 (1981).

[3]A. S. Goldhaber, Phys. Lett. 53B, 306 (1974).

[4]L. M. Anderson, Ph. D. thesis, Lawrence Berkeley Laboratory Report No. LBL 6769, 1977; T. Fujita and J. Hüfner, Nucl. Phys. A 343, 493 (1980).

[5]P. J. Lindstrom, D. E. Greiner, H. H. Heckman, B. Cork, and F. S. Bieser, Lawrence Berkeley Laboratory Report No. LBL 3650 (unpublished).

[6]J. Hüfner and M. C. Nemes, Phys. Rev. C 23, 2538 (1981).

[7]V. F. Weisskopf, Nucl. Phys. 3, 423 (1957).

[8]B. G. Harvey, Phys. Rev. Lett. 47, 454 (1981); D. K. Scott *et al.*, Lawrence Berkeley Laboratory Report No. 7729, 1978 (unpublished).

[9]For the fragment ^{14}O an additional spectroscopic factor of 0.5 has been included to account for the fact that one of the two low-lying 0^+ states is above the decay threshold, while for ^{14}C both are below threshold.